Ferrocenylethynylbenzenes as Precursors to in Situ Synthesis of Carbon Nanotube and Fe Nanoparticle Compositions

Teddy M. Keller* and Syed B. Qadri†

Chemistry and Materials Science and Technology Divisions, Naval Research Laboratory, Washington, D.C. 20375

Received October 3, 2003. Revised Manuscript Received December 22, 2003

Several ferrocenyl-aryl-acetylenic compounds were synthesized and thermally converted in situ to carbon nanotube−Fe nanoparticle compositions. Upon melting, the ferrocenyl compounds are cured to a shaped configuration through the acetylenic units. Further heating of the polymeric composition results in the decomposition of the ferrocene and the ultimate formation of Fe nanoparticles. During the carbonization process above 500 °C in an inert atmosphere, the Fe nanoparticles react with the developing carbon nanoparticles resulting in the formation of carbon nanotubes in high yield within the carbonaceous media. Various shaped carbonaceous forms (solid, fiber, and film) containing large amounts of carbon nanotubes can be readily formulated from the precursor ferrocenyl compounds. The polymeric and carbonaceous compositions were characterized by thermogravimetric analysis (TGA) and differential scanning calorimetric analysis (DSC), X-ray diffraction, Raman, and high-resolution scanning electron microscopy (HRSEM) studies.

Introduction

Carbon nanotubes (CNTs) have attracted a great deal of interest due to their unique chemical and physical properties and major implications for industrial and technological applications.[1] In particular, solid or shaped carbon nanotube compositions with a small dispersion of metal nanoparticles are quite desirable as they can possess interesting electrical,[2,3] magnetic,[4,5] and mechanical[6,7] properties. Various synthetic methods such as arc discharge,[8,9] pulsed laser vaporization,[10,11] and chemical vapor deposition (CVD)[12−15] have been developed for the formulation of CNTs. None of these synthetic methods ensures a continuous, large-scale production of CNTs. The arc discharge and pulsed laser methods produce CNTs in low yield, are difficult to scale to industrial production levels, and contain large amounts of metal particles that are difficult to remove. The CVD method is superior to the other methods in terms of purity, yield, and alignment of the CNTs. Thus, numerous groups are focused on the improvement of the CVD technique for the preparation of vertically aligned CNTs.

The possibility of using organometallic compounds as precursors to CNTs, CNT−metal nanoparticle compositions, and nanocomposites is very attractive.[6,7,16−18] To date, little attention has been focused on developing polymeric precursors containing transition metals and the thermal conversion of such organometallic compounds into shaped components as precursors to CNTs. The presence of organometallic moieties in precursor compounds and linear polymers containing inorganic units have been shown to produce materials that possess excellent processability and solubility with enhanced thermal and oxidative stability and magnetic properties upon thermal treatment at elevated temperatures.[19−21]

* To whom correspondence should be addressed. E-mail: keller1@ccs.nrl.navy.mil. Chemistry Division.
† Materials Science and Technology Division.

(1) Ajayan, P. M. *Chem. Rev.* **1999**, *99*, 1787.
(2) Pascual, J. I.; Méndez, J.; GómezHerrero, J.; Baro, A. M.; Garcia, N.; Landman, U.; Luedtke, W. D.; Bogachek, E. N.; Cheng, H. P. *Science* **1995**, *267* (5205), 1793.
(3) Collins, P. G.; Zettl, A.; Bando, H.; Thess, A.; Smalley, R. E. *Science* **1997**, *278* (5335), 100.
(4) Dong, X. L.; Zhang, Z. D.; Jin, S. R.; Sun, W. M.; Zhao, X. G.; Li, Z. J.; Chuang, Y. C. *J. Mater. Res.* **1999**, *14* (5), 1782.
(5) Zhang, Z. D.; Zheng, J. G.; Skorvanek, I.; Wen, G. H.; Kovac, J.; Wang, F. W.; Yu, J. L.; Li, Z. J.; Dong, X. L.; Jin, S. R.; Liu, W.; Zhang, X. X. *J. Phys.: Condens. Matter* **2001**, *13* (9), 1921.
(6) Calvert, P. *Nature* **1999**, *399* (6733), 210.
(7) Ajayan, P. M.; Schadler, L. S.; Giannaris, C.; Rubio, A. *Adv. Mater.* **2000**, *12*, 750.
(8) Iijima, S.; Ichihashi, T. *Nature* **1993**, *363*, 603.
(9) Bethune, D. S.; Kiang, C. H.; de Vries, M. S.; Gorman, G.; Savoy, R.; Vazquez, J.; Beyers, R. *Nature* **1993**, *363*, 605.
(10) Guo, T.; Nikolaev, P.; Thess, A.; Colbert, D. T.; Smalley, R. E. *Chem. Phys. Lett.* **1995**, *243*, 49.
(11) Maser, W. K.; Muoz, E.; Benito, A. M.; Martnez, M. T.; de la Fuente, G. F.; Maniette, Y.; Anglaret, E.; Sauvajol, J. L. *Chem. Phys. Lett.* **1998**, *292*, 587.
(12) Peigney, A.; Laurent, C.; Dobigeon, F.; Rousset, A. J. *J. Mater. Res.* **1997**, *12*, 613.
(13) Hafner, J. F.; Bronikowski, M. J.; Azamiam, B. R.; Nikolaev, P.; Rinxler, A. G.; Colbert, D. T.; Smalley, R. E. *Chem. Phys. Lett.* **1998**, *296*, 195.
(14) Kitayananan, B.; Alvarez, W. E.; Harwell, J. H.; Resasco, D. E. *Chem. Phys. Lett.* **2000**, *317*, 497.
(15) Cassell, A. M.; Raymakers, J. A.; Kong, J.; Dai, H. *J. Phys. Chem. B* **1999**, *103*, 6484.
(16) MacLachlan, M. J.; Ginzburg, M.; Coombs, N.; Coyle, T. W.; Raju, N. P.; Gredan, J. E.; Ozin, G. A.; Manners, I. *Science* **2000**, *287*, 1460.
(17) Ozin, G. A. *Adv. Mater.* **1992**, *4*, 612.
(18) Jiles, D. *Introduction to Magnetism and Magnetic Materials*; Chapman and Hall: London, 1991; p 69.
(19) Houser, E. J.; Keller, T. M. *Macromolecules* **1998**, *31*, 4038.
(20) Corriu, R. J. P.; Devylder, N.; Guerin, C.; Henner, B.; Jean, A. *J. Organomet. Chem.* **1996**, *509*, 249.

10.1021/cm030624e
Published on Web 02/26/2004

The incorporation of a variety of metal units into a compound or polymer is a synthetic challenge. Our approach for the homogeneous incorporation of metal nanoparticle involves the synthesis of melt-processable organometallic compounds containing ethynyl units for both polymerization purposes and a site for complexation of transition metals. Ferrocene-based materials were used in our studies because of their stability and the low cost of ferrocene. When heated above 300 °C, ferrocene is known to decompose, leading initially to Fe atom formation.[22] Our initial efforts involve the reaction of ethynylferrocene with bromoiodobenzene or diiodobenzene followed by end-capping with either ethynylferrocene or ethynylbenzene. In essence, this method gives us the ability to control the amount of Fe incorporated into the precursor compounds. These compounds **4** and **5**, upon thermal treatment up to and above 500 °C, result in the formation initially of Fe atoms and ultimately Fe nanoparticles uniformly dispersed in the resulting cross-linked polymeric and carbonaceous domains.[22,23] The viscosity of the melt at a given temperature will control the diffusive properties of the individual metal particles in the polymerizing matrix. The size and interparticle separation of the Fe atoms/nanoparticles will be controlled in the melt state above 300 °C. Upon gelation, the mobility of the Fe particles will be greatly reduced. The beauty of this approach is that shaped components or films can be readily fabricated from the melt or liquid state of the precursor compounds. The matrix domain has the ability to control the size and shape of the growing Fe nanparticle and to protect it against oxidation. In the present studies, the in situ formation of CNTs in high yield from melt-processable ferrocenylalkynylaromatic compounds **4** and **5** that are heated to elevated temperatures will be described. The CNT−Fe nanoparticle compositions were characterized by thermogravimetric analysis, X-ray diffraction, Raman, and high-resolution scanning electron microscopy (HRSEM) studies.

Experimental Section

All synthetic reactions were performed under argon using standard Schlenk line techniques. Reagent grade solvents were dried using standard methods and distilled under argon prior to use. Ethynylferrocene, **1**, was prepared according to the published procedures.[24] $Pd(OAc)_2$ was purchased from Strem Chemical Co. and was used as received. All other chemicals were purchased from Aldrich Chemical Co. and were used as received. Product separations were performed by column chromatography using 200−400 mesh, 60-Å silica gel. Thermogravimetric analyses (TGA) and differential scanning calorimetric (DSC) analyses were performed on a TA SDT 2960 Simultaneous DTA−TGA module and a TA DSC 2920 modulated DSC, respectively, equipped with a TA 3100 thermal analyzer. All thermal analyses were performed using heating rates of 10 °C/min under a nitrogen atmosphere with flow rates of 100 cm^3/min. Melting points were determined by DSC analyses. Infrared spectra (FTIR) were recorded on a Nicolet Magna 750 spectrophotometer. ^1H NMRs were performed on a Brüker AC-300 spectrometer. Elemental analyses were performed by Galbraith Laboratories, Inc. X-ray analyses were performed using a Rigaku 18 kW X-ray generator and a high-resolution powder diffractometer. X-ray diffraction scans of the samples were measured using Cu Kα radiation from a rotating anode X-ray source. Raman spectroscopy was carried out at room temperature using a Renishaw Raman spectrometer equipped with a 514.5-nm argon laser. High-resolution scanning electron microscopy (HRSEM) was performed using a LEO 1550.

General Procedure for the Palladium-Catalyzed Cross-Coupling Reactions. A 50-mL round-bottomed flask equipped with a magnetic stirrer and gas inlet was purged with argon and charged with the appropriate aryl halide and terminal alkyne, 5 mol % $Pd(OAc)_2$ and 15 mol % PPh_3. A 5:1:1 (v/v) tetrahydrofuran/pyridine/diisopropylamine solvent mixture was added via syringe, and the mixture was then stirred at room temperature for 20 min. CuI (1−2.5 mol %) was then added, and the reaction mixture was placed in a dry ice/acetone bath (−78 °C). The mixture was then evacuated and backfilled with argon several times, warmed to room temperature, and stirred for 16 h at 25 or 60 °C for the aryl iodide or aryl bromide, respectively, with the progress of the reaction being monitored by ^1H NMR. Upon completion of the reaction, the mixture was filtered through Celite, the volatiles were removed in vacuo, and the product was separated by flash chromatography on silica gel.

Synthesis of 1-(Ferrocenylethynyl)-3-bromobenzene (3a). Compound **3a** was prepared following the general procedure for the palladium-catalyzed coupling reaction using 500 mg (2.38 mmol) of **1**, 642 mg (2.27 mmol) of 1-bromo-3-iodobenzene, 25.5 mg (0.114 mmol) of $Pd(OAc)_2$, 89.2 mg (0.341 mmol) of PPh_3, and 10.8 mg (0.0568 mmol) of CuI in 25 mL of tetrahydrofuran, 5 mL of pyridine, and 5 mL of diisopropylamine at 25 °C. The residue was purified using a 5:1 hexane/CH_2Cl_2 solvent mixture to afford 761 mg (92%) of an orange-red solid, mp 130 °C. Spectral data for **3a**. IR (cm^{-1}, KBr): 3094 (C−H), 3057 (C−H), 2218 (C≡C), 2204 (C≡C), 1591 (C═C, benzene), 1583 (C═C, benzene), 1552 (C═C, benzene), 1411 (C═C, ferrocene). ^1H NMR (δ in $CDCl_3$): 7.63 (t, J = 1.7 Hz, 1H), 7.41 (m, 2H), 7.17 (t, J = 7.8 Hz, 1H), 4.50 (t, J = 1.9 Hz, 2H), 4.25 (t, J = 1.9 Hz, 2H), 4.24 (s, 5H). Analysis for **3a** ($C_{18}H_{13}FeBr$) Calcd: C, 59.22%; H, 3.59%. Found: C, 59.15%; H, 3.84%.

Synthesis of 1-(Ferrocenylethynyl)-4-bromobenzene (3b). Compound **3b** was prepared following the general procedure for the palladium-catalyzed coupling reaction using 500 mg (2.38 mmol) of **1**, 641 mg (2.27 mmol) of 1-bromo-4-iodobenzene, 25.4 mg (0.114 mmol) of $Pd(OAc)_2$, 89.0 mg (0.340 mmol) of PPh_3, and 10.8 mg (0.0568 mmol) of CuI in 25 mL of tetrahydrofuran, 5 mL of pyridine, and 5 mL of diisopropylamine at 25 °C. The residue was purified using a 3:1 hexane/CH_2Cl_2 solvent mixture to afford 703 mg (85%) of an orange-red solid, mp 147 °C. Spectral data for **3b**. IR (cm^{-1}, KBr): 3104 (C−H), 3082 (C−H), 2218 (C≡C), 2205 (C≡C), 1496 (C═C, benzene), 1411 (C═C, ferrocene). ^1H NMR (δ in $CDCl_3$): 7.46−7.42 (m, 2H), 7.35−7.31 (m, 2H), 4.49 (t, J = 1.7 Hz, 2H), 4.24 (t, J = 1.7 Hz, 2H), 4.23 (s, 5H). Analysis for **3b** ($C_{18}H_{13}FeBr$) Calcd: C, 59.22%; H, 3.59%. Found: C, 59.22%; H, 3.76%.

Synthesis of 1-(Ferrocenylethynyl)-3-(phenylethynyl)-benzene (4a). Compound **4a** was prepared following the general procedure for the palladium-catalyzed coupling reaction using 500 mg (1.37 mmol) of **3a**, 210 mg (2.05 mmol) of phenylacetylene, 15.4 mg (0.0686 mmol) of $Pd(OAc)_2$, 53.9 mg (0.206 mmol) of PPh_3, and 2.6 mg (0.0137 mmol) of CuI in 25 mL of tetrahydrofuran, 5 mL of pyridine, and 5 mL of diisopropylamine at 60 °C. The residue was purified using a 5:1 hexane/CH_2Cl_2 solvent mixture to afford 442 mg (84%) of an orange-red solid, mp 181 °C. Spectral data for **4a**. IR (cm^{-1}, KBr): 3111 (C−H), 3097 (C−H), 2212 (C≡C), 1597 (C═C, benzene), 1570 (C═C, benzene), 1491 (C═C, benzene), 1411 (C═C, ferrocene). ^1H NMR (δ in $CDCl_3$): 7.67 (m, 1H), 7.53 (m, 2H), 7.44 (m, 2H), 7.34 (m, 3H), 7.29 (t, J = 7.8 Hz, 1H),

(21) Peterson, R.; Foucher, D. A.; Tang, B.-Z.; Lough, A.; Raju, N. P.; Greedan, J. E.; Manners, I. *Chem. Mater.* **1995**, *7*, 2045.
(22) Yusuda, H.; Hiwara, A.; Nakamura, A.; Sakai, H. *J. Inorg. Organomet. Polym.* **1991**, *1* (2), 239.
(23) Miyanagam S.; Yasuda, H.; Hiwara, A.; Nakumura, A. *J. Macromol. Sci.-Chem.* **1990**, *A27* (9−11), 1347.
(24) Doisneau, G.; Balavoine, G.; Fillebeen-Khan, T. *J. Organomet. Chem.* **1992**, *425*, 113.

4.50 (t, $J = 1.8$ Hz, 2H), 4.24 (m, 7H). Analysis for **4a** ($C_{26}H_{18}Fe$) Calcd: C, 80.84%; H, 4.70%. Found: C, 80.31%; H, 4.63%.

Synthesis of 1-(Ferrocenylethynyl)-4-(phenylethynyl)benzene (4b). Compound **4b** was prepared following the general procedure for the palladium-catalyzed coupling reaction using 500 mg (1.37 mmol) of **3b**, 210 mg (2.05 mmol) of phenylacetylene, 15.4 mg (0.0686 mmol) of $Pd(OAc)_2$, 53.9 mg (0.206 mmol) of PPh_3, and 2.6 mg (0.0137 mmol) of CuI in 25 mL of tetrahydrofuran, 5 mL of pyridine, and 5 mL of diisopropylamine at 60 °C. The residue was purified using a 5:1 hexane/CH_2Cl_2 solvent mixture to afford 385 mg (73%) of an orange-red solid, mp 198 °C. Spectral data for **4b**. IR (cm^{-1}, KBr): 3084 (C−H), 3056 (C−H), 2203 (C≡C), 1594 (C═C, benzene), 1517 (C═C, benzene), 1411 (C═C, ferrocene). ^1H NMR (δ in $CDCl_3$): 7.51 (m, 2H), 7.45 (m, 4H), 7.33 (m, 3H), 4.50 (t, $J = 1.9$ Hz, 2H), 4.24 (t, $J = 1.9$ Hz, 2H), 4.23 (s, 5H). Analysis for **4b** ($C_{26}H_{18}Fe$) Calcd: C, 80.84%; H, 4.70%. Found: C, 80.06%; H, 4.72%.

Polymerization and Carbonization of 1-(Ferrocenylethynyl)-3 or 4-(Phenylethynyl)benzene (4a or 4b) Resulting in the Formation of CNT−Fe Nanoparticle Compositions. Compounds **4a** (15.1 mg) and **4b** (16.2 mg) were weighed into a TGA boat and polymerized by heating under a nitrogen atmosphere at 225 °C for 5 min, at 300 °C for 30 min, and at 350 °C for 30 min, resulting in the formation of a solid thermosetting polymeric material. During the heat treatment, the samples from **4a** and **4b** lost about 12% and 15% of their weight, respectively. Upon cooling, the resulting thermosets from the polymerization reaction were heated in a TGA boat from 30 to 1000 °C at 10 °C/min under a nitrogen atmosphere affording char yields of 86% and 84%, respectively, resulting in the formation of CNTs−Fe nanoparticle compositions in high yield.

Synthesis of 1,3-Bis(Ferrocenylethynyl)benzene (5a). Compound **5a** was prepared following the general procedure for the palladium-catalyzed coupling reaction using 520 mg (2.48 mmol) of **1**, 389 mg (1.18 mmol) of 1,3-diiodobenzene, 13.3 mg (0.059 mmol) of $Pd(OAc)_2$, 46.4 mg (0.177 mmol) of PPh_3, and 5.6 mg (0.030 mmol) of CuI in 25 mL of tetrahydrofuran, 5 mL of pyridine, and 5 mL of diisopropylamine at 25 °C. The residue was purified using a 5:1 hexane/CH_2Cl_2 solvent mixture to afford 526 mg (82%) of an orange solid, mp 225 °C. Spectral data for **5a**. IR (cm^{-1}, KBr): 3103 (C−H), 3088 (C−H), 2215 (C≡C), 1594 (C═C, benzene), 1569 (C═C, benzene), 1410 (C═C, ferrocene). ^1H NMR (δ in $CDCl_3$): 7.61 (t, $J = 1.5$ Hz, 1H), 7.40 (dd, $J = 7.1$ Hz, $J = 1.5$ Hz, 2H), 7.26 (t, $J = 7.1$ Hz, 1H), 4.50 (t, $J = 1.9$ Hz, 4H), 4.24 (m, 14H). Analysis for **5a** ($C_{30}H_{22}Fe_2$) Calcd: C, 72.91%; H, 4.49%. Found: C, 72.42%; H, 4.69%.

Synthesis of 1,4-Bis(Ferrocenylethynyl)benzene (5b). Compound **5b** was prepared following the general procedure for the palladium-catalyzed coupling reaction using 500 mg (2.38 mmol) of **1**, 314 mg (0.952 mmol) of 1,4-diiodobenzene, 10.7 mg (0.0476 mmol) of $Pd(OAc)_2$, 37.3 mg (0.143 mmol) of PPh_3, and 3.6 mg (0.019 mmol) of CuI in 25 mL of tetrahydrofuran, 5 mL of pyridine, and 5 mL of diisopropylamine at 25 °C. The residue was purified using a 2:1 hexane/CH_2Cl_2 solvent mixture to afford 343 mg (73%) of an orange solid, mp 257 °C. Spectral data for **5b**. IR (cm^{-1}, KBr): 3099 (C−H), 3080 (C−H), 2224 (C≡C), 2202 (C≡C), 1519 (C═C, benzene), 1411 (C═C, ferrocene). ^1H NMR (δ in $CDCl_3$): 7.41 (s, 4H), 4.49 (t, $J_{H-H} = 3.3$ Hz, 4H), 4.24 (m, 14H). Analysis for **2b** ($C_{30}H_{22}Fe_2$) Calcd: C, 72.91%; H, 4.49%. Found: C, 72.46%; H, 4.61%.

Polymerization and Carbonization of 1,3- or 1,4-Bis(Ferrocenylethynyl)benzene (5a or 5b) Resulting in the Formation of CNT−Fe Nanoparticle Compositions. Compounds **5a** (16.8 mg) and **5b** (13.7 mg) were weighed into a TGA boat and polymerized by heating under a nitrogen atmosphere at 225 °C for 5 min, at 300 °C for 30 min, and at 350 °C for 30 min, resulting in the formation of a solid, black thermosetting polymeric material. During the heat treatment, the samples from **5a** and **5b** lost about 11% and 16% of their weight. The resulting thermosets from the polymerization reaction were cooled and heated in a TGA boat from 30 to 1000 °C at 10 °C/min under a nitrogen atmosphere affording char yields of 90% and 88%, respectively, resulting in the formation of CNTs−Fe nanoparticle compositions in high yield.

Results and Discussion

CNT Synthesis in Bulk Composition. We have developed a novel method for the formation of CNTs in bulk solid compositions starting with ferrocenyl-aryl-acetylenic compounds. Ferrocenyl-aryl-acetylenic compounds **4** and **5** that have low melting points and have a broad processing window, defined as the temperature difference between the melting point and the exothermic polymerization reaction, can be easily polymerized through the acetylenic units to a shaped component (solid, film, and fiber). The ultimate size and separation of the Fe nanoparticles is dependent on the time to gelation at a given temperature and whether decomposition of the ferrocene moiety occurs in the melt phase or after solidification. Heat treatment of a composition above 500 °C results in the formation of Fe nanoparticles and the initiation of the carbonization process. The Fe nanoparticles interact with the developing carbon nanoparticles causing the formation of CNTs. As the temperature is increased, the rate of carbon nanotubes growth is enhanced. X-ray diffraction studies show the initial formation of very small carbon nanoparticles that react with the Fe nanoparticles causing conversion to CNT−Fe nanoparticle compositions during the heat treatment to elevated temperatures. This process is controlled as a function of the temperature and the time of exposure.

This method using ferrocenyl units as the source of Fe nanoparticles in the precursor compound and leading to the formation of CNTs allows for an inexpensive chemical synthesis of carbon nanotubes in large quantities, in high yield, and in a shaped configuration. The key to the formation of the carbon nanotube compositions is the formation of the Fe nanoparticles from degradation of the ferrocenyl unit. The rate of formation, yield at any given time, and average size of the CNTs in the pyrolysis process is dependent on the temperature, size of the Fe nanoparticle, and the time of temperature exposure.

Carbonization Process and Formation of Carbon Nanotubes. During the carbonization process, the Fe atoms and/or Fe nanoparticles directly aid in the formation and the size of CNTs. The mechanisms for the formation of CNTs formed during carbonization of compositions from **4** and **5** and by the current methods[25−32] are probably different. The CNTs of our unique method are formed in the solid phase and are

(25) Iijima, S.; Ichihashi, T. *Nature* **1993**, *363*, 603.
(26) Bethune, D. S.; Kiang, C. H.; de Vries, M. S.; Gorman, G.; Savoy, R.; Vazquez, J.; Beyers, R. *Nature* **1993**, *363*, 605.
(27) Guo, T.; Nikolaev, P.; Thess, A.; Colbert, D. T.; Smalley, R. E. *Chem. Phys. Lett.* **1995**, *243*, 49.
(28) Maser, W. K.; Muoz, E.; Benito, A. M.; Martnez, M. T.; de la Fuente, G. F.; Maniette, Y.; Anglaret, E.; Sauvajol, J. L. *Chem. Phys. Lett.* **1998**, *292*, 587.
(29) Peigney, A.; Laurent, C.; Dobigeon, F.; Rousset, A. J. *J. Mater. Res.* **1997**, *12*, 613.
(30) Hafner, J. F.; Bronikowski, M. J.; Azamiam, B. R.; Nikolaev, P.; Rinxler, A. G.; Colbert, D. T.; Smalley, R. E. *Chem. Phys. Lett.* **1998**, *296*, 195.
(31) Kitayananan, B.; Alvarez, W. E.; Harwell, J. H.; Resasco, D. E. *Chem. Phys. Lett.* **2000**, *317*, 497.
(32) Cassell, A. M.; Raymakers, J. A.; Kong, J.; Dai, H. *J. Phys. Chem. B* **1999**, *103*, 6484.

not produced from gaseous carbon components as is common with the current methods of preparation. Our studies indicate that small carbon nanoparticles are initially formed at approximately 600 °C. The carbon nanoparticles are the building blocks to the formation of CNTs.

During the pyrolysis of **4** and **5**, a progressive increase in the formation of polycondensed ring structures occurs during the polymerization reaction involving initially the alkynyl units.[33−36] As the heat treatment is continued at higher temperatures, thermal decomposition occurs producing free radicals accompanied by limited polycondensation of the aromatic ring and followed by orientation of polycondensed rings in a fixed direction.[36] By accumulation of oriented polycondensed aromatic layers, small carbon nanoparticles are formed by pairing of the free radicals.[36−38] The developing polycondensed ring structures and/or carbon nanoparticles apparently react with the Fe atoms and/or nanoparticles to initiate the CNT growth process. It has been observed[39] that CNTs are formed only when the diameter of the metal catalytic particle is below 40 nm.

As the Fe nanoparticle−carbon system is heated from 600 to 1400 °C, the conversion and yield of CNTs rapidly increase. The rate of formation and conversion of the carbon nanoparticles within the carbonaceous media to CNTs occurs expeditiously as the temperature is increased. In a system with a low concentration of Fe nanoparticles, longer exposure times at a given temperature would be necessary for high conversion to CNTs. During curing and heat treatment to 1400 °C, the retention of weight was 70−80%, and the composition has been mainly converted to CNTs surrounded by some amorphous carbon. The shaped compositions from heat treatment of **4** and **5** have structural integrity, which enhances their importance for potential fibrous and matrix composite applications.

Synthesis of Ferrocenyl Compounds. Our synthetic strategy for preparing the ferrocenyl compounds used in our studies involves disubstituted benzenes bearing two ferrocenylethynyl groups or a combination of one ferrocenylethynyl and one phenylethynyl group. Modification of the synthetic method being used allows for controlling the amount of ferrocenyl units, which is important for varying the concentration and size of the Fe nanoparticles and ultimately the formation of CNT compositions. Smaller molecules are desirable due to the ability to process shaped components from a melted form. The synthetic procedure allows us not only to vary the amount of Fe in our materials, but also to alter the melting point through the preparation of the aromatic isomers, resulting in some control in the size of the processing window. Studies have been previously reported[19,40] in our laboratory on the synthesis, polymerization, and pyrolysis of acetylene-substituted aromatic and Fe containing compounds.

Scheme 1. Synthesis of Ferrocenylethynylbenzenes 4a, 4b, 5a, and 5b

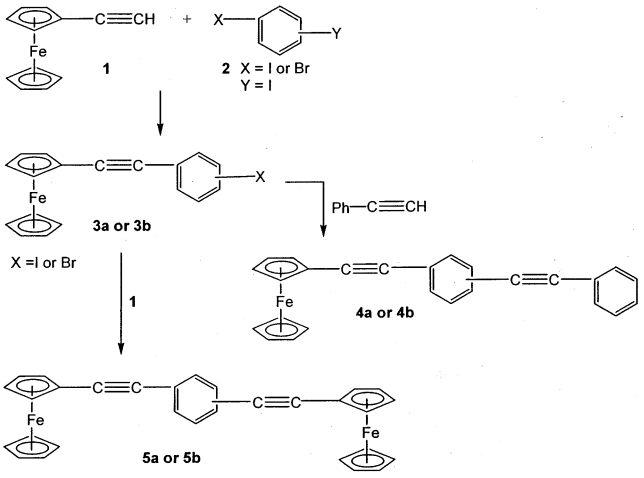

The ferrocenyl-aryl-acetylene compounds **4** and **5** were prepared as shown in Scheme 1. One or two equivalents of ethynylferrocene **1** and the appropriate bromoiodobenzene or diiodobenzene, respectively, are mixed initially at −78 °C in the presence of a solvent mixture of THF/diisopropylamine/pyridine and a catalytic amount of $Pd(OAc)_2$, PPh_3, and CuI. The reaction mixture is then degassed and backfilled with argon several times before warming to room temperature. 1,3-Bis(ferrocenylethynyl)benzene **5a**, 1,4-bis(ferrocenylethynyl)benzene **5b**, 1-(ferrocenylethynyl)-3-bromobenzene **3a**, and 1-(ferrocenylethynyl)-4-bromobenzene **3b** were prepared from the palladium/copper-mediated cross-coupling reaction in 82, 73, 92, and 85%, respectively. The slightly lower yield observed for **5b**, was attributed to solubility difficulties during purification by column chromatography. Subsequently, 1-(ferrocenylethynyl)-3-(phenylethynyl)benzene **4a** and 1-(ferrocenylethynyl)-4-(phenylethynyl)benzene **4b** were prepared from the reaction of the appropriate brominated benzene **3** with phenylacetylene in yields of 84 and 73%, respectively. The synthesis of **5b** was previously reported from the reaction of ethynylferrocene and 1,4-diiodobenzene in high yield (94%).[41] However, the compound was not fully characterized, and attempts to reproduce the results in similar yield were unsuccessful.

Thermal Analyses. Studies pertaining to the processability and decomposition of **4a**, **4b**, **5a**, and **5b** resulting in the formation of CNTs and Fe nanoparticles were determined using thermal analysis. To obtain a shaped structure or film, it is important that the compounds melt. Differential scanning calorimetry (DSC) is extremely valuable in determining the processing window between the melting point of the compound and the polymerization temperature. Figure 1 shows the DSC thermograms for the compounds heated to 400 °C. The melting points (endotherm) for **4a**, **4b**, **5a**, and **5b** are at 181, 198, 225, and 257 °C. The polymerization reaction (cure, peak exotherm) to a cross-linked system (thermoset) involves the ethynyl moieties and occurs at

(33) Berris, B. C.; Hovakeemian, G. H.; Lai, Y.-H.; Mestdagh, H.; Vollhardt, K. P. C. *J. Am. Chem. Soc.* **1985**, *107*, 5670.
(34) Hirthammer, M.; Vollhardt, H. P. C. *J. Am. Chem. Soc.* **1986**, *108*, 2481.
(35) Diercks, R.; Vollhardt, K. P. C. *J. Am. Chem. Soc.* **1986**, *108*, 3150.
(36) Honda, H. *Carbon* **1988**, *26* (2), 139.
(37) Bruck, S. D. *Polymer* **1965**, *6*, 319.
(38) Fitzer, E. *Pure Appl. Chem.* **1980**, *52*, 1865.
(39) Gavillet, J.; Loiseau, A.; Ducastelle, F.; Thair, S.; Bernier, P.; Stéphan, O.; Thibault, J.; Charlier, J.-C. *Carbon* **2002**, *40*, 1649.
(40) Jones, K. M.; Keller, T. M. *Polymer* **1995**, *36* (1), 187.
(41) Rodriguez, J. G.; Onate, A.; Martin-Villamil, R. M.; Fonseca, I. *J. Organomet. Chem.* **1996**, *513*, 71.

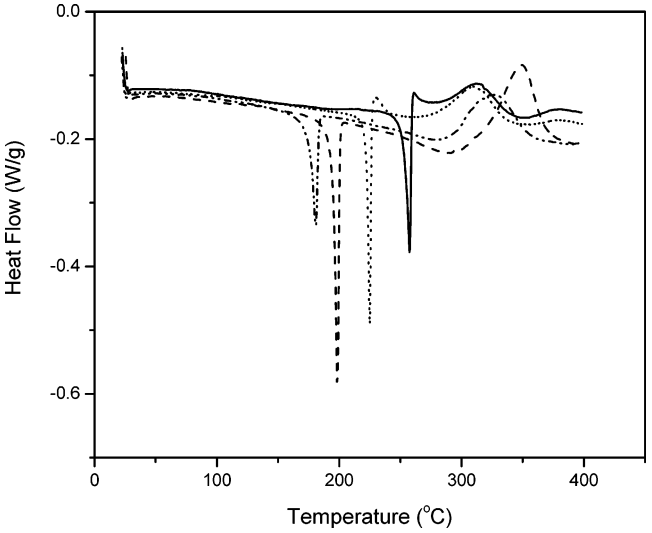

Figure 1. DSC thermograms of ferrocenylethynylbenzenes: **4a** [– · ·], **4b** [– –], **5a** [· · ·], and **5b** [solid].

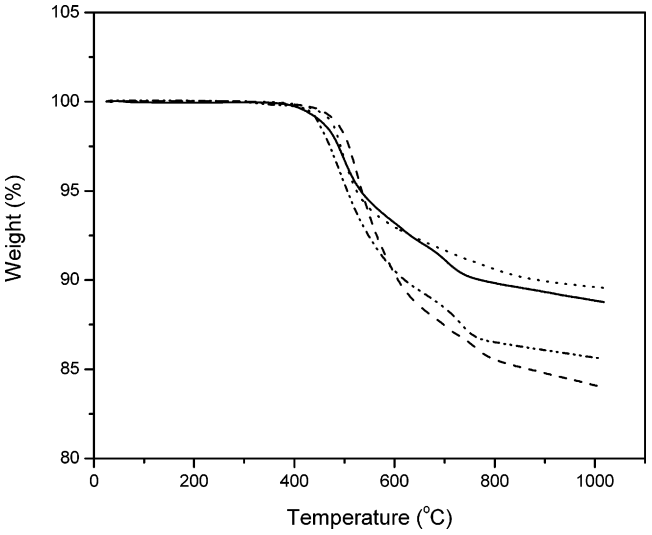

Figure 2. TGA thermograms of ferrocenylethynylbenzenes: **4a** [– · ·], **4b** [– –], **5a** [· · ·], and **5b** [solid].

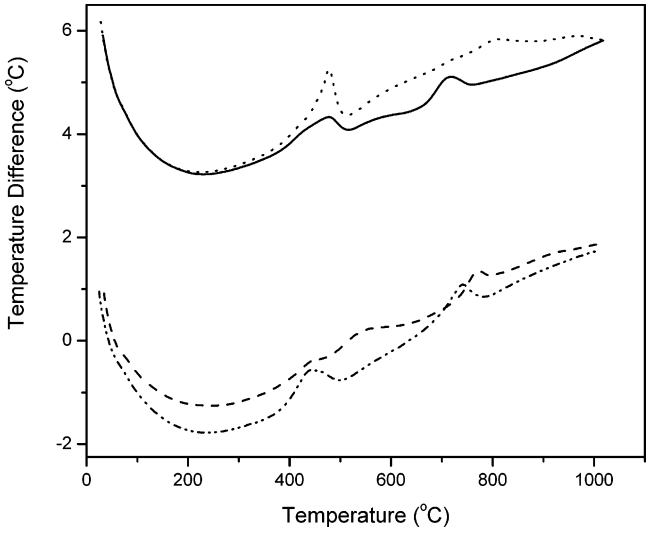

Figure 3. DTA thermograms of ferrocenylethynylbenzenes: **4a** [– · ·], **4b** [– –], **5a** [· · ·], and **5b** [solid].

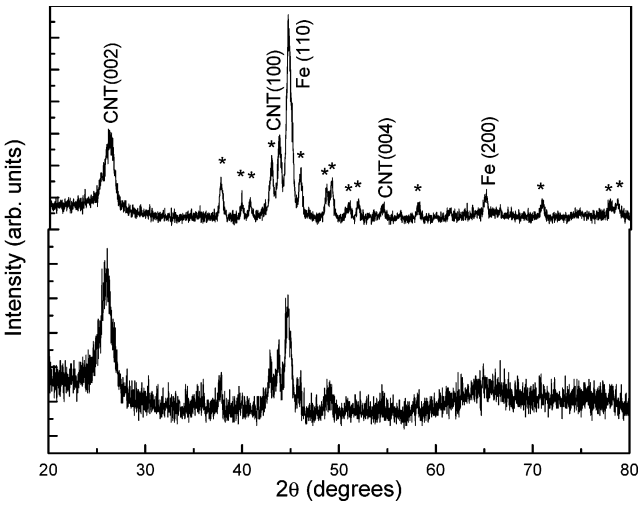

Figure 4. X-ray diffraction scans for **4b** (bottom) and **5a** (top).

325, 350, 310, and 313 °C, respectively. Compound **5b** has a short processing window and actually commences to cure during the melt process.

The thermal stability of**4a**, **4b**, **5a**, and **5b** was determined by TGA–DTA analyses by heating each sample at 10 °C/min under a nitrogen atmosphere up to 1000 °C (Figures 2 and 3). The thermal analyses were performed on samples that had been converted to a thermoset by heating at 300 and 350 °C for 30 min at each temperature. Further heating of the thermosets to 1000 °C under nitrogen affords CNT–Fe nanoparticle carbon compositions in 85–90% char yield (Figure 2). Because of the presence of the Fe nanoparticles dispersed in the CNTs–Fe nanoparticle domains, the carbonaceous compositions are attracted to a permanent magnet indicating ferromagnetic behavior.

Figure 3 shows the differential thermal analysis (DTA) thermograms on the thermosets from **4a**, **4b**, **5a**, and **5b** that were heated to 1000 °C. These thermograms are useful for determining endothermic and exothermic transitions occurring during thermal treatments to elevated temperatures. Thermosets formed from **4a**, **4b**, **5a**, and **5b** displayed an exothermic transition peaking at 445, 441, 478, and 479 °C, respectively, which is believed due to the decomposition of the ferrocene moiety. The appearance of another exothermic transition peaking at approximately 741, 773, 807, and 722 °C was assigned to reaction of the Fe nanoparticles with the developing carbon nanoparticle matrix[42] resulting in the formation of carbon nanotubes based on X-ray diffraction studies. To show the importance and necessity of the Fe atoms and/or Fe nanoparticles in the formation of the CNTs, a nonferrocene-containing compound, 1,2,4,5-tetrakis(phenylethynyl)benzene, upon thermal treatment to 1000 °C, did not exhibit these transitions or result in the formation of carbon nanotubes.

X-ray Diffraction Studies. X-ray diffraction scans of the samples were taken using Cu Kα radiation from a rotating anode X-ray source. The samples were finely ground and mounted on a Si (001) substrate. To avoid the silicon substrate peak and to minimize the background, the ω-angle was offset by 6°. Figure 4 shows the scans for samples designated as **4b** and **5a**. All the diffraction peaks have been identified and indexed on

(42) Yasuda, H.; Hiwara, A.; Nakamura, A.; Sakai, H. *J. Inorg. Organmet. Polym.* **1991**, *1*, 239.

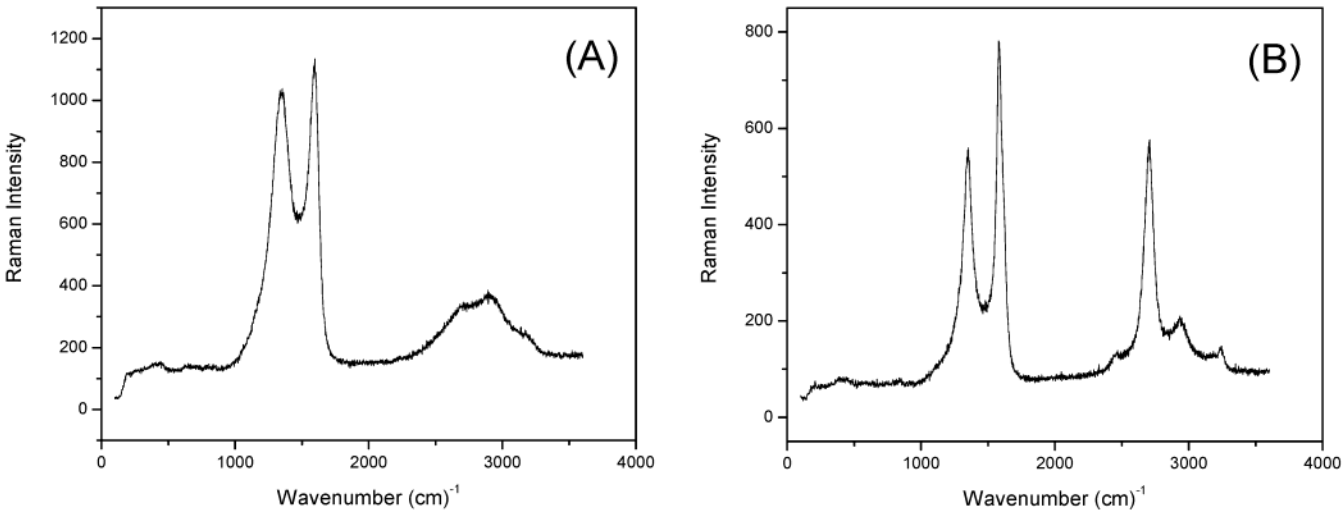

Figure 5. Raman spectra of (A) **4a** and (B) **5b**.

Table 1. X-ray Diffraction Data (in nm) on 4a, 4b, 5a, and 5b Heated to 1000 °C

sample	*c*-lattice parameter	CNT (diameters)	Fe (particle size)
4a	0.686	6.10	20.4
4b	0.681	6.00	15.1
5a	0.682	6.75	16.1
5b	0.683	6.05	17.5

the basis of carbon nanotubes (graphite-like), α-Fe, and Fe_3C phases. The particle sizes were estimated from the full width at half-maximum (fwhm) of the diffraction peaks using the Scherrar's equation.[43] The lattice parameters for α-Fe and Fe_3C phases were in good agreement with their corresponding bulk values. The peaks at 2θ angle of 25.97, 43.5, and 58.5 degrees are attributed to the structure of carbon nanotubes (CNT), which have a graphite-like structure.[44] These peaks were fitted to a hexagonal unit cell and lattice parameters of $a = 0.245 \pm 0.005$ nm and $c = 0.684 \pm 0.005$ nm were obtained. The diameters of carbon nanotubes were obtained using the fwhm of CNT (002) and Scherrar's formula. The occurrence of these peaks in an X-ray scan serves as the fingerprint for the presence of carbon nanotubes.

The ratio of peak intensities of CNT (002) and α-Fe (110) was very much dependent on the Fe content in the precursor material, whereas the shift in the CNT (002) was nearly independent. Pyrolyzed samples from **5a** and **5b**, which had similar Fe-content, showed identical diffraction patterns in which the α-Fe (110) peak was much stronger than the CNT (002) peak. Heat-treated samples from **4a** and **4b** had a lower Fe content and their diffraction patterns showed a much stronger CNT (002) peak in comparison with the Fe (110) peak, indicating the presence of a large amount of carbon nanotubes. Furthermore, the Fe_3C phase was substantially reduced when compared to the bcc Fe phase. The particle sizes and the *c*-lattice parameters for CNTs are all listed in Table 1.

Raman Studies. Raman measurements were performed on the surface of the CNT-containing solids prepared by the novel method using a 514.5-nm argon laser. In these studies, Raman spectra were obtained and compared with highly aligned, purified CNTs previously prepared by carbon arc discharge method.[45−48] The temperature-induced growth of nanotubes in the bulk sample was analyzed in terms of the change in the width and relative intensity of the first-order D and G peaks (first-order Raman), which lie at about 1347 and 1575 cm^{-1}, respectively, and the second-order scattering peaks between 2450 and 3250 cm^{-1}. In **5a** and **5b**, the peaks of the first- and second-order spectra were sharp, indicating an increase in the uniformity of the CNTs and lower levels of carbon impurity relative to **4a** and **4b**. Figure 5 shows the Raman spectra of **4a** and **5a** heated to 1000 °C. The CNTs were more highly developed on the surface of **5** relative to those of **4** as determined by the development of the first- and second-order peaks.

The radial breathing modes at low frequency were of extremely low intensity or missing in the Raman spectra (Figure 5). The radial breathing mode (RBM) present near 200 cm^{-1} in the current CNTs is directly related to the diameter of SWNTs and can be estimated from the formula $\omega = 223.75/d$ where d is the diameter of the CNTs and ω is the frequency of the radial breathing mode in wavenumber.[46,49] According to this formula, peaks present at 192 and 254 cm^{-1} would correspond to SWNTs with diameters of 1.16 and 0.88 nm, respectively. Yudasaka[50] has reported difficulty in observing the RBM peaks for SWNTs with a diameter greater than 2 nm. Using this formula and our X-ray results, CNTs formed in our studies with diameters of approximately 6.0 nm would show RBM peaks at about 37.29 cm^{-1}, which explains the absence of the peaks in

(43) Cullity, B. D. *Elements of X-ray Diffraction*; Addison-Wesley: Reading, PA, 1978; p 102.
(44) Dobiasova, L.; Stary, V.; Glogar, P.; Valvoda, V. *Carbon* **1999**, *37*, 421.
(45) Hiuri, H.; Ebbesen, T. W.; Tanigaki, K.; Takahashi, H. *Chem. Phys. Lett.* **1993**, *202* (6), 509.
(46) Rao, A. M.; Richter, E.; Bandow, S.; Chase, B.; Eklund, P. C.; Williams, K. A.; Fang, S.; Subbaswamy, K. R.; Menon, M.; Thess, A.; Smalley, R. E.; Dresselhaus, R. E.; Dresselhaus, M. S. *Science* **1997**, *275*, 187.
(47) Li, W.; Zhang, H.; Wang, C.; Zhang, Y.; Xu, L.; Zhu, K.; Xie, S. *Appl. Phys. Lett.* **1997**, *70* (20), 2684.
(48) Fang, S. L.; Rao, A. M.; Eklund, P. C.; Nikolaev, P.; Rinzler, A. G.; Smalley, R. E. *J. Mater. Res.* **1998**, *13* (9), 2405.
(49) Xiaohong, L.; Zhang, J.; Li, Q.; Li, H.; Liu, Z. *Carbon* **2003**, *41*, 579.
(50) Yudasaka, M.; Ichihashi, T.; Kasuya, D.; Kataura, H.; Iijima, S. *Carbon* **2003**, *41*, 1273.

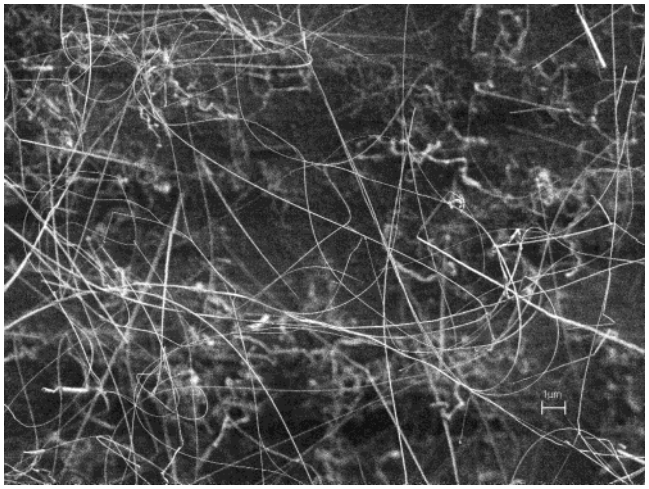

Figure 6. Compound **5a** was melted onto the surface of a silicon wafer and heated to 1000 °C. The bulk solid CNT composition failed to adhere to the silicon. HRSEM analysis of film remaining on surface of silicon wafer showed long horizontal CNT strands or nanfilaments.

the Raman spectra. Previous heat-treatment studies on SWNTS from 1000 to 1700 °C have shown the formation of larger SWNTs (2−4 nm) from coalescence with neighbors at higher temperatures, which has been demonstrated to be an effective way to enlarge the diameter of CNTs.[48−51] The larger SWNTs did not show RBM peaks in the Raman spectra. Moreover, in bulk compositions where the spectra are a superposition of numerous contributions from various CNTs of different diameters, broad unresolvable features have previously[46,52] been observed in the low-frequency range.

High-Resolution Scanning Electron Microscopy (HRSEM) Studies. HRSEM images were obtained on a film that remained on the surface of a silicon wafer by melting and heating a sample of **5a** to 1000 °C. The pyrolyzed solid sample containing the CNTs failed to adhere to the silicon wafer. Upon removal of the bulk solid, a thin film had formed on the silicon wafer where the solid CNT composition had been. HRSEM analysis (Figure 6) of the film shows long individual CNT strands or nanofilaments in an isotopic array. The observed larger diameter of the CNT strands relative to the bulk solid (Table 1) could occur from CNT coalescence with neighbors at higher temperatures or could be multiwalled CNTs. The average diameter of an individual strand was measured to be 42.7 nm. The resulting strands have a wide distribution of radial sizes. The lengths of most strands are greater than 20 μm. The length and diameter of the CNTs probably depend on the growth duration and heat treatment at the elevated temperature. It appears that bundles containing CNTs of smaller diameter are also formed beneath the larger strands and nearer the surface of the silicon. Previous studies on pure SWNTs have shown that the structure was not greatly changed when exposed to heat treatment up to 800 °C.[50,51] As the temperature was increased, the diameter size of SWNTs increased up to 1600 °C. Above 1600 °C, the SWNTs were converted into MWNTs.[50]

Conclusion

To be useful for electronic and structural applications, it is important that the formation of CNT and metal nanoparticle compositions by thermal means occurs with minimum loss of weight. Organometallic compounds or transition-metal-containing polymers that exist in the liquid state or melt are a promising route to CNTs and processable metal nanoparticle compositions. The properties of the composition can be tailored depending on the quantity of CNTs to metal nanoparticles. Ferrocenylethynyl compounds were used in these studies as precursors to CNT and Fe nanoparticle polymeric and carbon compositions. TGA/DTA studies show an exothermic transition for the precursors **4** and **5** peaking between 722 and 807 °C, which is believed due to the reaction of the Fe particle with the developing carbon nanoparticles to produce CNTs. Further studies are underway to determine the thermal effect and concentration of metal moiety in precursor organometallic compounds on the formation of CNTs−metal nanoparticle compositions and the resulting physical properties.

Acknowledgment. The Office of Naval Research (ONR) is acknowledged for financial support of this work. We thank Joseph L. Perrin for the initial synthesis of the ferrocenyl acetylenic-containing compounds used in this study. Joseph L. Perrin was an American Society for Engineering Education (ASEE)/ONR Postdoctoral Fellow.

CM030624E

(51) Méténier, K.; Bonnamy, S.; Béguin, F.; Journet, C.; Bernier, P.; de La Chapelle, M. L.; Chauvet, O.; Lefrant, S. *Carbon* **2002**, *40*, 1765.

(52) Duesberg, G. S.; Blau, W. J.; Byrne, H. J.; Muster, J.; Burghard, M.; Roth, S. *Chem. Phys. Lett.* **1999**, *310*, 8.